EM Waveguides

Ismael Leal

March 2023

1 Introduction

Throughout the twentieth century electrical communication systems were being developed, which led to the creation of microwave communication systems, operating at bit rates (a measure of the speed with which information is being sent) of around 100 MB/s. It was later realised that the bit rate could be increased by some orders of magnitude if an optical wave (higher frequency) was used as carrier instead. The invention of LASER technology in 1960 allowed the idea of light confinement, suggesting optical fibers as a good choice for guiding light. By 2001, a bit rate of 10 Tb/s was achieved [Agrawal, 2010, p.2-16].

Optical fibers are nothing but dielectric waveguides. In other words, they are structures that have the purpose of guiding the waves' energy transmission, whether EM or sound waves. They are designed to minimise the loss of energy: without waveguides, the energy of these waves decreases with the square of the distance. The first used waveguides were conductive metal pipes, which can be used to transport microwaves, mainly. However, dielectric waveguides (particularly optical fibers) provide a way to confine light. Using them, energy and information loss can be incredibly minimised for communications. It is thanks to waveguides that almost-instantaneous telecommunications exist. As such a relevant part of this century's technology, the study of waveguides is of utmost importance.

Nevertheless, many real-world scenarios are too complicated to obtain an exact analytical solution to describe them. Scientific computing has been helpful against this deterrent to the physical sciences. Compared to humans, computers have a far greater processing speed and capacity to find numerical approximations to problems without exact analytical solutions. Concerning waveguides, the propagation of electric and magnetic fields through space would require a massive amount of calculations to predict how light would behave inside an optical fiber. Luckily, some numerical methods can be used to predict these scenarios.

In this report, the Finite Difference Time-Domain (FDTD) method will be used to simulate an optical fiber. Fourier theory will be used to perform a mode analysis of a straight optical fiber, decomposing the frequencies and analysing the dispersion relationships for every mode inside the fiber. Finally, the simulation will show the fiber performing a 90-degree right turn. A relationship for the intensity loss as a function of the curvature radius will be obtained.

2 Theoretical framework

2.1 Finite Difference Time Domain technique and implementation

2.1.1 General information

Historically, predictions for EM waves have been made through experiments or theoretical understanding. Computational predictions have been made possible in the last years through the use of numerical methods. FDTD is one of the most used numerical methods for EM waves, as it can be easily applied to a wide range of situations.

The advantages of FDTD are countless. To begin with, it can simulate arbitrary geometries and predict how light will interact with them, which is not an easy task without FDTD. It works with a wide range of frequencies and can simulate stimuli such as RADAR, LASER, High Power Microwaves, ... Also, its accuracy can be set as high as required just by using a large enough number of spatial and temporal steps.

Drawbacks of FDTD include its computational cost. It is not exceeding, but a large number of cells or a large number of time steps will result in a slower software. Thus, only small physical systems will be studied.

2.1.2 Mathematical development

FDTD is based on Faraday's law and Ampere-Maxwell Law in their derivative form. Through central finite differences (which have a lower error than forward and backward differences), the derivatives in Maxwell's equations are approximated as subtractions. The central difference has the following expression

$$\left.\frac{\partial f(x)}{\partial x}\right|_{x_k} \approx \frac{f(x_{k+1}) - f(x_{k-1})}{2\Delta x} \tag{1}$$

As the wave equation has second derivatives, an expression for the second-order derivative of a function $f(x)$ needs to be obtained:

$$\left.\frac{\partial^2 f(x)}{\partial x^2}\right|_{x_k} = \frac{1}{2\Delta x}\left(\left.\frac{\partial f(x_{k+1})}{\partial x}\right|_{x_k} - \left.\frac{\partial f(x_{k-1})}{\partial x}\right|_{x_k}\right) \tag{2}$$

Applying backward and forward differences respectively, a final expression for solving differential equations can be obtained:

$$\left.\frac{\partial^2 f(x)}{\partial x^2}\right|_{x_k} = \frac{f(x_{k+1}) - 2f(x_k) + f(x_{k-1})}{2\Delta x^2} \tag{3}$$

This equation suggests that when applying this approximation to a derivative that differentiates with respect to a variable α, then α should be discretised. The software built is a 2-D simulation, so we'll work with the wave equation for 2-D where c is the wave speed.

$$\frac{\partial^2 f}{\partial t^2} = c^2\left(\frac{\partial^2 f}{\partial x^2} + \frac{\partial^2 f}{\partial y^2}\right) \tag{4}$$

As there are second derivatives with respect to three coordinates, 2-D space and time will be discretised, and the notation $f(x_i, y_j, t_n) \equiv f^n(i,j)$ will be adopted. Now the second-order derivative approximation from Equation 3 can be applied to Equation 4

$$\frac{f^{n+1}(i,j) - 2f^n(i,j) + f^{n-1}(i,j)}{2\Delta t^2} = c^2\left(\frac{f^n(i+1,j) - 2f^n(i,j) + f^n(i-1,j)}{2\Delta x^2} + \frac{f^n(i,j+1) - 2f^n(i,j) + f^n(i,j-1)}{2\Delta y^2}\right) \tag{5}$$

Then,

$$\begin{aligned} f^{n+1}(i,j) = &\left(\frac{c\Delta t}{\Delta x}\right)^2 (f^n(i+1,j) - 2f^n(i,j) + f^n(i-1,j)) \\ &+ \left(\frac{c\Delta t}{\Delta y}\right)^2 (f^n(i,j+1) - 2f^n(i,j) + f^n(i,j-1)) + 2f^n(i,j) - f^{n-1}(i,j) \end{aligned} \tag{6}$$

and an update equation has been obtained. This allows the value for the next discretised time step (immediate future) to be found in terms of present and past values. Also, notice only nearest neighbours are used for the calculations of each cell, making the FDTD technique not so computationally expensive.

Now, an update wave equation like Equation 6 can be obtained specifically for EM waves. Consider Maxwell equations for isotropic, linear, nondispersive material without sources. Faraday and Ampere-Maxwell laws in terms of electric field $\mathbf{E}$ and magnetic field $\mathbf{H}$ [Griffiths, 1999, p.321]:

$$\begin{cases} \nabla \times \mathbf{E} = -\frac{\partial \mathbf{B}}{\partial t} = -\mu\frac{\partial \mathbf{H}}{\partial t} \\ \frac{1}{\mu}\nabla \times \mathbf{B} = \nabla \times \mathbf{H} = \epsilon\frac{\partial \mathbf{E}}{\partial t} \end{cases} \tag{7}$$

Applying the curl to both sides of both Equations 7, using the identity $\nabla \times \nabla \times \mathbf{F} \equiv -\nabla^2 \mathbf{F} + \nabla (\nabla \cdot \mathbf{F})$, and taking into account that the other Maxwell equations when there are no sources state that $\nabla \cdot \mathbf{E} = \nabla \cdot \mathbf{H} = 0$:

$$\begin{cases} \nabla^2 \mathbf{E} = \mu\epsilon \frac{\partial^2 \mathbf{E}}{\partial t^2} \\ \nabla^2 \mathbf{H} = \mu\epsilon \frac{\partial^2 \mathbf{H}}{\partial t^2} \end{cases} \tag{8}$$

These are uncoupled, second-order wave equations, i.e., they take the form of Equation 4 where the wave speed is $\frac{1}{\sqrt{\mu\epsilon}} = \frac{c}{\sqrt{\mu_r \epsilon_r}}$, where c is the speed of light $c = (\mu_0 \epsilon_0)^{-1/2}$. As they are vector equations, we can extract an equation for each component. For this 2-D software, we assume that the fields only vary along two dimensions ($\frac{\partial}{\partial z} = 0$). These two vector equations give 6 equations, and we can separate them into two self-consistent sets of solutions, which are two different polarisations. The z-component of the first equation, and the x- and y- components of the second equation in Equations 8, are a set of independent equations showing E_x, E_y, andH_z:

$$\begin{cases} \frac{\partial H_z}{\partial y} = \epsilon \frac{\partial E_x}{\partial t} \\ \frac{\partial H_z}{\partial x} = -\epsilon \frac{\partial E_y}{\partial t} \\ \frac{\partial E_y}{\partial x} - \frac{\partial E_x}{\partial y} = -\mu \frac{\partial H_z}{\partial t} \end{cases} \tag{9}$$

It can be seen that Equations 9 refer to the modes where the H-field is parallel to the z-direction and the E-field is contained within the xy-plane. Hence, these are the TE_z modes, i.e. modes with the E-field transverse to the z-direction (note that the simulated 2-D waveguide will be parallel to the xy-plane, so that they will be referred to as TM modes later, where the magnetic field is perpendicular to the direction of propagation). Note that for these modes, H_z carries all the information, as it determines the two other components E_x and E_y. Had the other TM_z modes been chosen, then E_z would carry all the information.

Now apply central differences for the spatial derivatives, and forward differences for time derivatives. This has been chosen so that the future values of E_x, E_y, and H_z can be obtained in terms of the present values. Equations 9 now look like the following:

$$\begin{cases} \frac{H_z^n(i,j+1) - H_z^n(i,j-1)}{2\Delta y} = \epsilon \frac{E_x^{n+1}(i,j) - E_x^n(i,j)}{\Delta t} \\ \frac{H_z^n(i+1,j) - H_z^n(i-1,j)}{2\Delta x} = -\epsilon \frac{E_y^{n+1}(i,j) - E_y^n(i,j)}{\Delta t} \\ \frac{E_y^n(i+1,j) - E_y^n(i-1,j)}{2\Delta x} - \frac{E_x^n(i,j+1) - E_x^n(i,j-1)}{2\Delta y} = -\mu \frac{H_z^{n+1}(i,j) - H_z^n(i,j)}{\Delta y} \end{cases} \tag{10}$$

from which, solving for the future values, the update equations for the software have been obtained. For the software, $\Delta x = \Delta y \equiv \Delta s$:

$$\begin{cases} H_z^{n+1}(i,j) = H_z^n(i,j) + \frac{1}{\mu} \frac{\Delta t}{2\Delta s} \left[\left(E_x^n(i,j+1) - E_x^n(i,j-1)\right) - \left(E_y^n(i+1,j) - E_y^n(i-1,j)\right) \right] \\ E_x^{n+1}(i,j) = E_x^n(i,j) + \frac{1}{\epsilon} \frac{\Delta t}{2\Delta s} \left[H_z^n(i,j+1) - H_z^n(i,j-1) \right] \\ E_y^{n+1}(i,j) = E_y^n(i,j) - \frac{1}{\epsilon} \frac{\Delta t}{2\Delta s} \left[H_z^n(i+1,j) - H_z^n(i-1,j) \right] \end{cases} \tag{11}$$

2.1.3 Yee cells

In 1966, Kane Yee published "Numerical solution of initial boundary value problems involving maxwell's equations in isotropic media", where he proposed an idea that gave FDTD an opportunity to flourish and be much more useful. He proposed staggering the spatial and time components in such a way that the set of finite difference equations 11 are easily applicable [Yee, 1966]. In subsection 2.1.4, the specific choice for said

staggering will be described, but the basic idea is placing E_x, E_y, and H_z in an orientation that allows the derivatives to be approximated as central differences. This is an improvement, as central differences have a lower error than forward/backward differences, which were also used in Equations 11, so these are not the final version of the update equations yet.

2.1.4 Software implementation

Creation of the animation explain x,y, indexing, pyplot pcolormesh and what it needs

Numerical stability The condition for stability is that the EM field varies slightly between adjacent cells, without significantly large changes. As such, a grid length $\Delta s \sim \lambda$ would not satisfy this criterion. A variable called S in the software was given a value of 10, making sure that the grid length Δs is at least 10 times smaller than the shortest wavelength of the simulation.

The stability criterion is given by Yee, 1966:

$$\sqrt{(\Delta x)^2 + (\Delta y)^2} = \sqrt{2\,(\Delta s)^2} = \sqrt{2}\Delta s > c\Delta t \tag{12}$$

or

$$\Delta t < \frac{\sqrt{2}\Delta s}{c} \tag{13}$$

As long as Equation 13 is true, the stability condition is met. Accordingly, Δt was set to be $\Delta t = N\frac{\Delta s}{c0}$, where $N < \sqrt{2}$. A safe upper-bound limit for N was $\frac{1}{\sqrt{2}} \approx 0.7$, and it was finally set to 1/3 (note $1/3 < \sqrt{2}$).

Yee cells & array implementation As explained, Yee came up with an idea that allowed easier and better calculations of the EM fields. The main idea is to allow for central differences with respect to both space and time.

Here I will describe the specific choice for said staggering that was implemented into the software. In order to allow for all derivatives to be central, notice how in Equations 11, the next value of E_x in time depends on its nearest H_z neighbours in the y-direction. Similarly, the next E_y value depends on its nearest H_z neighbours in the x-direction. However, H_z values depend on the nearest E_x neighbours in the y-direction and the nearest E_y neighbours in the x-direction. Hence, the distribution in Figure 1 was adopted.

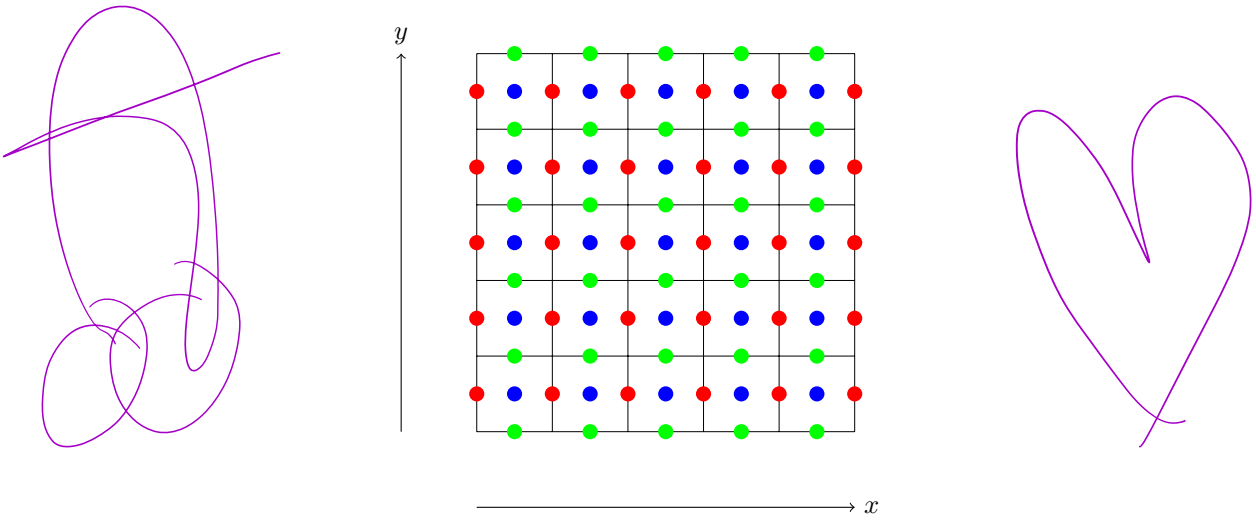

Figure 1: Suitable distribution for EM fields staggering (Red: E_y; Green: E_x; Blue: H_z)

Tracing back to Equations 11, the central differences that were applied to spatial derivatives can be easily calculated now.

This spatial staggering is surely helpful, however achieving update equations through central time differences too would be ideal. Yee proposed discretising time so that E_x and E_y time values coincide, and H_z is calculated for in-between time steps. Thus, what before was $H_z^n(i,j)$ now it's $H_z^{n+\frac{1}{2}}(i+\frac{1}{2},j+\frac{1}{2})$ and $H_z^{n-1}(i+\frac{1}{2},j+\frac{1}{2})$ is now $H_z^{n-\frac{1}{2}}(i+\frac{1}{2},j+\frac{1}{2})$

Considering everything, the final update equations look like this:

$$\begin{cases} H_z^{n+\frac{1}{2}}(i+\frac{1}{2},j+\frac{1}{2}) = H_z^{n-\frac{1}{2}}(i+\frac{1}{2},j+\frac{1}{2}) + \frac{1}{\mu}\frac{\Delta t}{\Delta s}\left[\begin{array}{l}\left(E_x^n(i+\frac{1}{2},j+1) - E_x^n(i+\frac{1}{2},j)\right) \\ -\left(E_y^n(i+1,j+\frac{1}{2}) - E_y^n(i,j+\frac{1}{2})\right)\end{array}\right] \\ E_x^{n+1}(i+\frac{1}{2},j) = E_x^n(i+\frac{1}{2},j) + \frac{1}{\epsilon}\frac{\Delta t}{\Delta s}\left[H_z^{n+\frac{1}{2}}(i+\frac{1}{2},j+\frac{1}{2}) - H_z^{n+\frac{1}{2}}(i+\frac{1}{2},j-\frac{1}{2})\right] \\ E_y^{n+1}(i,j+\frac{1}{2}) = E_y^n(i,j+\frac{1}{2}) - \frac{1}{\epsilon}\frac{\Delta t}{\Delta s}\left[H_z^{n+\frac{1}{2}}(i+\frac{1}{2},j+\frac{1}{2}) - H_z^{n+\frac{1}{2}}(i-\frac{1}{2},j+\frac{1}{2})\right] \end{cases} \tag{14}$$

Notice that some indices have changed, but due to the specific staggering, all of the differences are central, minimising error and allowing for easy calculations.

Array implementation The array indices have to be chosen carefully so that Yee cells actually work. This poses a computational problem as the values for the EM fields need to be stored in arrays, and there are no half-indices in arrays. Thus, Yee cells will be created. These would be 3-D cells (in x, y, and time) for our 2-D software.

As the software was created in Python, the EM field values were stored in Numpy arrays, so that the y-indices go from 0 (top row) to the maximum value (bottom row), and the x-indices go from 0 (left column) to the maximum value (right column). Therefore, the Yee cell with indices (i,j) at time step n covers t_n and $t_{n-\frac{1}{2}}$, and includes $E_x^n(i+\frac{1}{2},j)$, $E_y^n(i,j-\frac{1}{2})$, and $H_z^{n-\frac{1}{2}}(i+\frac{1}{2},j-\frac{1}{2})$. All the indices for the Yee cells are integers, so now the staggering shown in Figure 1 is ready to be implemented.

The code for the update equations 14 would then be:

- Hz_nplus1[1:ny-1,1:nx-1] = Hz_n[1:ny-1,1:nx-1] + (dt / (mu*ds))*((Ex_n[0:ny-2,1:nx-1] - Ex_n[1:ny-1,1:nx-1]) - (Ey_n[1:ny-1,2:nx] - Ey_n[1:ny-1,1:nx-1]))]
- Ex_nplus1[1:ny-1,1:nx-1] = Ex_n[1:ny-1,1:nx-1] + (dt / (eps*ds))*(Hz_nplus1[1:ny-1,1:nx-1] - Hz_nplus1[2:ny,1:nx-1])
- Ey_nplus1[1:ny-1,1:nx-1] = Ey_n[1:ny-1,1:nx-1] - (dt / (eps*ds))*(Hz_nplus1[1:ny-1,1:nx-1] - Hz_nplus1[1:ny-1,0:nx-2])

Absorbing boundary conditions

2.2 Total Internal Reflection

2.2.1 Critical angle

Total Internal Reflection (TIR) is a phenomenon occurring when light incident on a less dense medium reaches the interface at a certain angle. The minimum angle at which light is fully reflected, i.e., the minimum angle for TIR is called the critical angle and can be calculated using **Snell's law** like

$$\theta_c = \arcsin\left(\frac{n_t}{n_i}\cdot\sin\theta_t\right) = \arcsin\left(\frac{n_t}{n_i}\right) \tag{15}$$

where n_t and n_i are the refractive indices of the transmitted and incident materials respectively, and θ_t is the transmitted angle, $\theta_t = \frac{\pi}{2}$ for TIR.

2.2.2 Energy transmission

Before studying waveguides, the software will be checked. The justification for testing the software through TIR comes from its significance in waveguides. Without TIR, not even light incident at large angles would totally reflect, resulting in a constant loss of field amplitudes, and hence in a loss of the information being transmitted.

To test the simulator, the ratio of transmitted energy to incident energy is calculated for a plane wave crossing an interface between two materials. The plane wave comes from an excitation of H_z and E_y for all the points in a vertical line. The excitation applied has the shape of a Gaussian derivative in time:

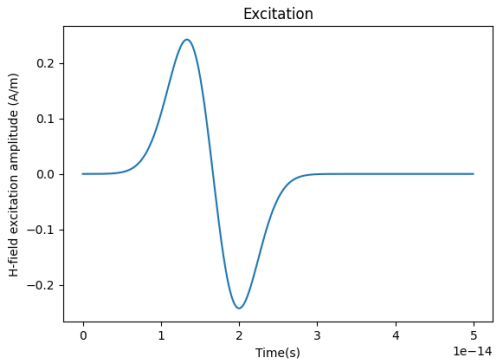

Figure 2: Excitation for a vertical plane wave pulse

For that purpose, the flux of the Poynting vector $\left(\vec{S} = \vec{E} \times \vec{H}\right)$ is calculated over two surfaces, one before the interface (S1) and another one after the interface (S2), giving the power across the surfaces. These values are then added for each time iteration, giving the total energy crossing each surface.

Both surfaces are taken in the y-z plane, so that they look as vertical lines in the x-y plane for the 2-D simulation. The differential surface term for the flux integrals is then given by:

$$\vec{dA} = \hat{n}dA = \begin{pmatrix} 1 \\ 0 \\ 0 \end{pmatrix} dA \tag{16}$$

Therefore, only the x-component of the Poynting vector contributes, and it is given by $S_x = E_y H_z - E_z H_y = E_y H_z$, because E_z and H_y are both 0 in the simulation (only TM modes are considered). Then, by adding $E_y \cdot H_z$ for every spatial point and every time iteration at each of both surfaces, the ratio can be obtained:

$$\frac{E_{transmitted}}{E_{incident}} = \frac{\int \left(\iint_{S1} \vec{S}\vec{dA}\right) dt}{\int \left(\iint_{S2} \vec{S}\vec{dA}\right) dt} = \frac{\int \left(\iint_{S1} E_y H_z dy dz\right) dt}{\int \left(\iint_{S2} E_y H_z dy dz\right) dt} \approx \frac{\sum_n \sum_j E_y^n\,(i1, j)\, H_z^n\,(i1, j)\, dy}{\sum_n \sum_j E_y^n\,(i2, j)\, H_z^n\,(i2, j)\, dy} \tag{17}$$

where in the last step an arbitrary length for the z-dimension of the surfaces has been assumed to be 1, and the integrals with respect to y and t have been approximated by a sum.

2.3 Waveguides

The choice of material for optical fibers, in general for dielectric waveguides, totally determines whether light will be confined or not, the number of excited modes, ... It determines all aspects of how the wave will be guided.

Usually, optical fibers consist of a core through which light is guided, and a cladding material surrounding the core. A common core material is silica, usually doped with some material. For this simulation, germanium dioxide (GeO2) will be taken as the core, having a refractive index of $n_{core} = 1.55$ [Clayton and Simpson, 1987 p.1187-1188].

bold

The cladding helps confining the light within the core, protects the core from external damage, and reduces the signal's distortion. The most used material as cladding is pure silica (SiO2), with a refractive index of $n_{cladding} = 1.45$ [Ghatak and Thyagarajan, 1997]. Fluorinated Ethylene Propylene (FEP) is a relatively new cladding material with some advantages with respect to pure silica. It has a very low thermal expansion coefficient, and a refractive index of $n_{cladding} = 1.34$ [Wei et al., 2017, p.11348-11354]. Its lower refractive index makes it easier for the optical fiber to confine light. This will be the material used as cladding in the simulation.

As specified in Section 2.1.2, the FDTD method is applied to a two-dimensional scenario in this report. Therefore, the waveguides simulated will behave as infinite slab waveguides. These consist of a planar slab (core) with a higher refractive index than the surrounding cladding to allow for TIR, and have infinite width in one dimension, perpendicular to the propagation direction of light [Marcuse, 1989].

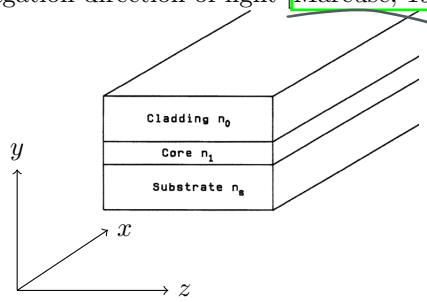

Figure 3: Slab waveguide, where the z-direction would be infinite in the simulation [Okamoto, 2022, p.14]

The optical fiber analysis in this report has two different sections. First, a mode analysis will be performed on a straight slab optical fiber using Fourier theory. Then, a 90° turn of the optical fiber will be simulated, and the energy lost as a function of radius will be found, as well as another mode analysis to find out whether some modes are lost in the way. energy lost as a function of radius, mode analysis as a function of radius

2.3.1 Frequency decomposition, mode analysis

Signals are characterised by the range of frequencies over which the signal carries the energy, i.e. the information. The difference between the highest and lowest frequencies contained in the signal is called its bandwidth, and is a measure of the spectral contents of the signal. The frequencies contained within the signal are obtained through the one-dimensional Fourier transform (FFT) of the field in the time domain, according to Fourier analysis.

The one-dimensional FFT can be applied to the field in the spatial domain of the axis of the optical fiber instead of the time domain. This yields the reciprocal space composition of the propagating pulse, i.e. the wavenumber component in the direction of the optical fiber's axis for each mode. These modes feel a different effective refractive index n_{eff} which can be calculated. The theoretical results will be compared with the experimental ones in the FDTD simulator.

First, an expression for the height h of the optical fiber's core in terms of the number of modes wanted will be obtained. This way, the software can be set to simulate an optical fiber depending on the input number of modes desired.

Note $|\vec{k}| = k_0 \cdot n_{core} = \frac{\omega_0}{c_0} \cdot n_{core}$, where k_0 is the wavenumber assigned to the central frequency of the pulse in vacuum and c_0 is the light speed in vacuum.

Now, each mode has light rays at discrete values of the angle of incidence θ_i with respect to the normal to the interface between core and cladding. The specific angle of incidence of a mode m, $\theta_{i,m}$ determines its propagation constants along x and y. Figure 4 shows they are, respectively:

$$\begin{cases} \beta = k_x = |\vec{k}| \sin\theta_i = k_0 n_{core} \sin\theta_i \\ \kappa = k_y = |\vec{k}| \cos\theta_i = k_0 n_{core} \cos\theta_i \end{cases} \tag{18}$$

According to the independent set of equations 9, the H-field will be in the z direction, perpendicular to the direction of propagation in the xy-plane. Consequently, we will be dealing with TM modes. Taking

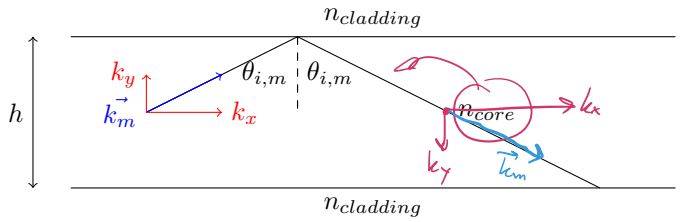

Figure 4: Profile of optical fiber

the reflection Fresnel coefficient for TM modes, the following expression for the phase shift can be obtained [Born and Wolf, 2013, p.36-41]:

$$\Phi = -2\tan^{-1}\left(\frac{\sqrt{\left(\frac{n_{core}}{n_{cladding}}\right)^2 \sin^2(\theta_i) - 1}}{\frac{n_{cladding}}{n_{core}}\cos(\theta_i)}\right) \tag{19}$$

Due to the finite length of the fiber in the y-direction, the allowed values of k_y are quantised. This is because only some of the values satisfy the given boundary conditions [Keiser, 2011, p.35-60]. Looking at the propagating mode in Figure 4, notice that the positive y-component of the first ray is equal and opposite to the negative y-component of the totally internally reflected second ray. This overlap forms what is known as a standing wave [Okamoto, 2022]. This vertical standing wave has undergone a certain phase shift known as Goos-Hänchen shift [Hecht, 2017]. Because the mode exists, the interference has to be constructive:

$$2hk_y + 2\Phi = 2m\pi \tag{20}$$

where m is any integer. Because the phase shift is small, the following simplification can be done:

$$k_y = \frac{2m\pi - 2\Phi}{2h} \approx \frac{2m\pi}{2h} = \frac{m\pi}{h} \tag{21}$$

So $k_y \propto m$, and Equation 35 shows that $k_y \propto \cos\theta_i$. Now, $\theta_i = \theta_c$ is the minimum angle of incidence of any existing, confined mode. Therefore, when θ_i is minimum at θ_c, $m = m_{max}$ is maximum.

So using Equations 15, 35, 21, and some trigonometric identities:

$$\boxed{h = \frac{\lambda_0 m_{max}}{2\sqrt{n_{core}^2 - n_{cladding}^2}}} \tag{22}$$

which is the Equation that will be used to obtain the necessary core height h depending on the number of modes wanted. This height will be used in the simulator to compare the FFT results with the theory.

Now that the height h can be set to allow a certain number of modes, a theoretical expression for the effective refractive index $n_{eff,m}$ of a mode m is needed to compare with the results of the Fourier analysis of the FDTD. These can be calculated simplifying Equation 20 and using the expression for Φ given by Equation 19:

$$\boxed{\frac{\sqrt{\left(\frac{n_{core}}{n_{cladding}}\right)^2 \sin^2(\theta_i) - 1}}{\frac{n_{cladding}}{n_{core}}\cos\theta} = \tan\left(\frac{hk_0 n_{core}\cos\theta_i - m\pi}{2}\right)} \tag{23}$$

Because m appears inside a tangent as $(-\frac{m\pi}{2})$, there will only be two different results, depending on whether it is even or odd. This equation will be the one used to calculate the theoretical values of θ_i for each mode. The total number of propagating modes should be equal to the total number of solutions both when m is odd and even.

However, Equation 23 can only be solved for θ_i numerically. Brent's method [**REFERENCE**] will be used to calculate the roots of:

$$f(\theta_i) = \frac{\sqrt{\left(\frac{n_{core}}{n_{cladding}}\right)^2 \sin^2(\theta_i) - 1}}{\frac{n_{cladding}}{n_{core}} \cos\theta} - \tan\left(\frac{hk_0 n_{core} \cos\theta_i - m\pi}{2}\right) = 0 \tag{24}$$

SciPy's built-in function "scipy.optimize.brentq(f, a, b)" [Scipy community, 2021] will be used to find the roots for Equation 24.

Finally, looking at Figure 4, the component of the wavevector in the direction of the waveguide's axis (the one returned by the FFT) is $k_x = \left(k_0 \cdot n_{core}\right) \cdot \sin\theta_i$. The effective refractive index of a mode can be calculated through:

$$k_x = k_0 \cdot n_{eff} \tag{25}$$

where k_0 is the wavenumber of the pulse in vacuum. Thus,

$$n_{eff,m} = \frac{k_x}{k_0} = n_{core} \cdot \sin\theta_i, m \tag{26}$$

subindex!

Given that the FFT returns k_x, then n_{eff} can be calculated both through Fourier analysis and using Equation 23 to obtain the angle of incidence.

experimentally

2.3.2 FFT2

FFT2: small temporal bandwidth so that there are many ωs "Fast Fourier Transform in Two Dimensions"

in-plane dispersion of a waveguide is important for signal processing and communications. Can optimise its design to minimise loss, high bandwidth

FFT2 of B-field profiles along waveguide in both space and time.

3 Total Internal Reflection

In this section, an analysis of the critical angle for different interfaces will be performed.

3.1 Software implementation

The setup consists of a vertical plane wave (propagating horizontally in the x-direction) incident in a diagonal interface, where the angle of incidence is the input determining the tilting of the interface.

To simulate the plane wave, the H_z and E_y fields of a vertical line (constant x-value) are excited with the shape of a Gaussian derivative in time (Figure 2). The relative permeability and permittivity are set as arrays. Because of the computational difficulty of simulating a tilted plane wave, the interface has to be tilted. It is modelled with the equation of a straight line of slope m calculated through $m = \frac{1}{\tan(\theta_i)}$, where θ_i is the desired angle of incidence with respect to the normal. All the spatial grid points to the right of said line are assigned the value of the permittivity and permeability of the second (transmitted) material. Similarly, all the grid points to the left of the interface are assigned the properties of the first (incident) material.

Some computational problems are encountered regarding the TIR. The plane wave is created as an infinite plane wave. The top and bottom ends of the plane wave do not diffract thanks to the fact that the software does not process the propagation of any wave outside of the boundaries, so it acts as if it was a perfect infinite plane wave. However, the plane wave is transmitted at the triple boundary between both materials and the bottom boundary of the simulation, and it is not supposed to refract at any point for $\theta_i \geq \theta_c$. It can be inferred that some intensity is "leaked" at that point and propagates through the second material. A screenshot of the animation shows the residual intensity being refracted into the second material.

The critical angle for the interface in Figure 5 can be calculated using Equation 15, $\theta_c = \arcsin\left(\frac{n_t}{n_i}\right) = \arcsin(1.34/1.55) = 60.00°$.

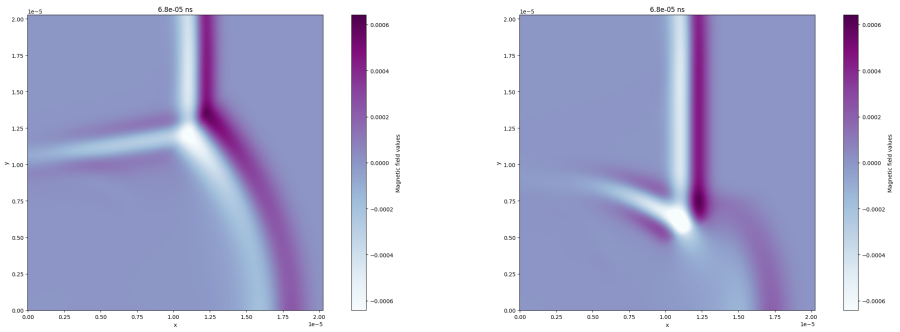

Figure 5: Infinite plane wave with an incidence of 35° (left) and 60° (right) from a material with $n_i = 1.55$ to a material of $n_t = 1.34$

Figure 5 shows that TIR is in fact working. The left image shows an incidence below the critical angle, and in the region near to the interface the refracted plane wave can be seen in the second material, where it later curves due to the "leaked" intensity from the bottom. The image on the right is supposed to show TIR. Now there is nothing resembling a plane wave in the transmitted region. The light at the other side of the interface looks as if it is propagating from the bottom corner, it doesn't look like a refracted plane wave.

Hence, the problem was a computational one, the physics were working. The next step was to restrict the plane wave vertically, so that light was not transmitted in said triple boundary. If the plane wave doesn't reach that point, the finite plane wave should be fully reflected. This only poses one problem, and it is the fact that, as the new plane wave does not behave as a perfect infinite one, the top and bottom points diffract a bit. This diffraction means that some light will be incident at angles smaller than the critical angle. The animation was then made larger to create a greater plane wave but still vertically finite, to reduce said diffraction. As expected, the top and bottom points refracted some light into the second material due to the curvature of the wave at those points and their lower angles of incidence. However, most of the wave is now perfectly reflected, as shown in Figure 6.

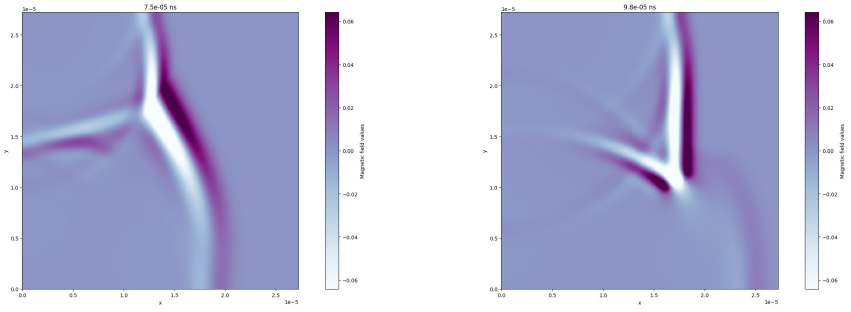

Figure 6: Finite plane wave with an incidence of 35° (left) and 60° (right) from a material with $n_i = 1.55$ to a material of $n_t = 1.34$

Similar to Figure 5, the left image of Figure 6 shows a transmitted plane wave after the interface while the right image shows TIR with the leaked intensity propagating in all directions. This is the setup used to measure the relative transmitted energy as a function of the angle of incidence.

3.2 Results

For the interface in Figure 7 the theoretical value of the critical angle is $\theta_c = 60.00°$, and it is the critical angle that will be used when simulating the optical fibers. According to Section 2.3, $n_{core} = n_i = 1.55$ and

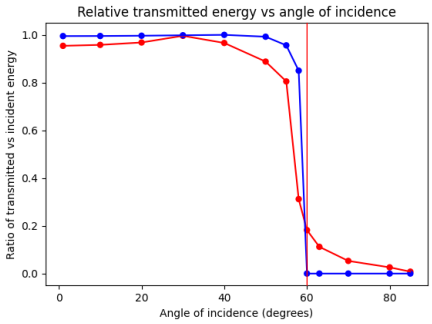

Figure 7: Relative transmitted energy; $\theta_c = 60.00°$ (blue: theoretical; red: experimental)

$n_{cladding} =$ 1.34. The intensity drops to almost 0 after showing an inflection point at the critical angle, although there is some intensity leaked due to the finite plane wave. There is a 5.30% of transmitted energy at $\theta_i = 70°$, and a 0.80% at $\theta_i = 85°$.

Hence, the transmitted residual energy to come from the diffracted ends of the wave, and so the software can be used to study waveguides: TIR works for angles of incidence greater than the critical angle.

4 Waveguides

bent waveguides: energy lost as a function of radius.

4.1 Software implementation

The simulation was created so that the user has the following inputs:

- The central frequency ω_0
- The frequency bandwidth σ_ω
- Refractive index of the core n_{core}
- Refractive index of the cladding $n_{cladding}$

The propagating pulse consists of an oscillating Gaussian excitation (Figure 8), defined by [Maclaurin, 1990 p.3275-3279]:

$$f(t) = \cos(\omega_0 t) \cdot \exp\left[-\frac{(t-t_0)^2}{2\sigma_t^2}\right] \tag{27}$$

where σ_t and t_0 are calculated from the user inputs as σ_ω^{-1} and $5\sigma_t$, respectively.

For the first part of this analysis where straight optical fibers will be simulated, the size of the simulation in the y-direction is reduced due to the simulated waveguide being parallel to the x-axis, so the extra space in the y-direction is not needed. This results in some reflection at the top and bottom limits of the simulation, due to the absorbing boundary conditions being an approximation.

As the waveguide in this part of the experiment is a straight one with its axis in the x-direction, the FFT of the field in the x-domain yields the component k_x shown in Figure 4.

Finally, because of the reduction in the y-direction size of the animation and the additional reflections that it creates, metallic walls were simulated to contain the radiation that leaves the waveguide because of its small angle of incidence. These walls block this noisy radiation from the excitation point and range from the outside of the core to the end of the simulation (Figure 9).

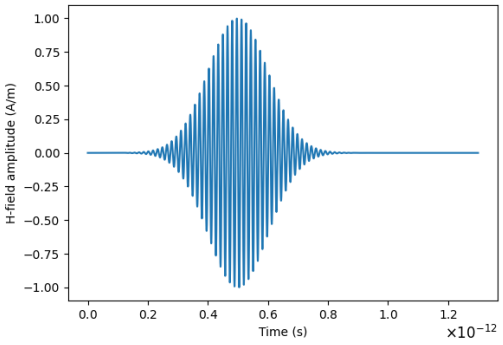

Figure 8: Excitation for an oscillating Gaussian pulse

4.1.1 Bent waveguides

In order to simulate the core of the waveguide performing a 90° turn, Boolean indexing was used. Boolean indexing allows the creation of Numpy masks, which in turn allow the software designer to modify the values of an array depending on a logical condition.

The arrays x and y are 2-D Numpy arrays storing the physical values, in meters, for the x- and y-positions respectively.

The 90° turn is a quarter of a circumference. Therefore, the bent waveguide can be parametrised as all the points within two concentric quarters of circumference, as **IMAGE CHATGPT LATEX BENT PART OF THE WAVEGUIDE**.

A Numpy mask can be created then that marks all points within the shaded area in Image **JAJAJ** as True, allowing the developer to modify only those values of the relative permittivity and permeability arrays. This results in effectively simulating a different material.

If this parametrisation is specified in terms of the desired physical radius of the quarter of circumference, then a waveguide where light propagates in the positive x-direction can be simulated performing a 90° turn so that light then propagates in the negative y-direction, as shown in Figure **OTRA CON UN DIBUJO DE LA WAVEGUIDE O LA MISMA PERO ENTONCES LA DE ANTES INCLUYENDO LAS PARTES RECTAS Y NO SOLO LA CIRCUMFERENCIA.**

4.2 Mode analysis

As mentioned in Section 2.3, the slab optical fiber simulated has a core of GeO2 ($n_{core} = 1.55$) and a FEP cladding ($n_{core} = 1.34$). These fibers are usually used for mid-infrarred (MIR) transmission, that has an associated central wavelength of $2 - 6\,\mu\text{m}$ [Henderson et al., 2006]. $\lambda_{core} = 3.00\,\mu\text{m}$ will be chosen. Using the conversion between wavelength and frequency, the necessary input central frequency can be determined:

$$\omega_0 = \frac{2\pi c}{\lambda_0} = \frac{2\pi c}{n_{core}\lambda_{core}} = 4.05 \times 10^{14}\,\text{rad} \cdot \text{s}^{-1} \tag{28}$$

where λ_0 is the vacuum wavelength. In order for the FFT to yield a wavelength distribution with a high resolution, the frequency bandwidth will be set as 40 times smaller than the central frequency:

$$\sigma_\omega = 0.1 \times 10^{14}\,\text{rad} \cdot \text{s}^{-1} \tag{29}$$

Therefore,

$$|k_{core}| = \frac{2\pi}{\lambda_{core}} \approx 2.09 \times 10^{6}\,\text{rad} \cdot \text{m}^{-1} \tag{30}$$

4.2.1 Single-mode optical fiber

First, a single-mode optical fiber ($m_{max} = 1$) will be simulated with the values shown in Equations 28, 29, 30. Using Equation 22

$$h = \frac{\lambda_{core} n_{core} m_{max}}{2\sqrt{n_{core}^2 - n_{cladding}^2}} = 3.00\,\mu\text{m} \tag{31}$$

Solving Equation 23 with Brent's method, a single solution of $\theta_i = 71.26°$ is obtained, so there is only one mode expected. This angle of incidence of the fundamental mode yields an expected value for k_x of:

$$k_x = |k_{core}| \sin\theta_i = 1.98 \times 10^6\,\text{rad} \cdot \text{m}^{-1} \tag{32}$$

which gives

$$\mathbf{n_{eff} = 1.47} \tag{33}$$

After applying the FFT to the field in the x-direction, the following results are obtained.

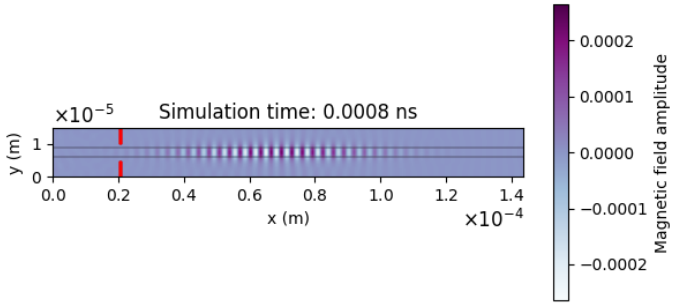

Figure 9: Screenshot of the pulse propagating through the described single-mode horizontal optical fiber

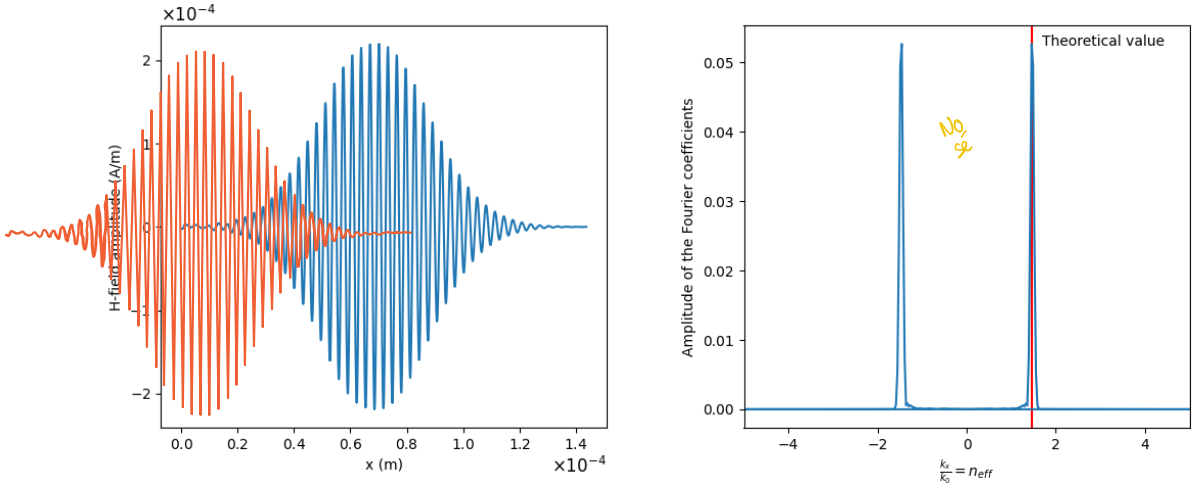

Figure 10: H_z value as a function of x in the fiber (left) and its FFT re-scaled to show the effective refractive index with a red line for the theoretical value (right)

Because of the reduction of the simulation in the y-direction, some residual reflections enter the optical fiber, but the metallic walls drawn in red in Figure 9 keep most this radiation to their left. However, some noise still re-enters the fiber and slightly modify the shape of Figure 10 (left) at small values of x. Still, the resolution of the peaks is high in the right plot, yielding only one main mode as expected, with a value of $k_x = 1.97 \times 10^6\,\mathrm{rad \cdot m^{-1}}$ rounded to 3 significant figures.

The achieved result through the FDTD method gives $\mathbf{n_{eff}} = \mathbf{1.46}$, which agrees with the theoretical value within a 0.68% error, which is really good.

4.2.2 2-mode optical fiber

For this sub-section, two modes will try to be obtained.

In order to simulate an optical fiber with two propagating modes, $m_{max} = 2$. The values shown in Equations 28, 29, 30, and Equation 22 allows the calculation of h:

$$h = \frac{\lambda_{core} n_{core} m_{max}}{2\sqrt{n_{core}^2 - n_{cladding}^2}} = 5.97\,\mu\mathrm{m} \tag{34}$$

Using Brent's method again to find the solution of Equation 23, two solutions are obtained (one for $m = 0$ and the other one for $m = 1$):

$$\begin{cases} \theta_{i,m=0} = 78.48^\circ \\ \theta_{i,m=1} = 67.44^\circ \end{cases} \tag{35}$$

These angles of incidence of both modes yield an expected value for k_x of:

$$\begin{cases} k_{x,m=0} = |k_{core}| \sin\theta_{i,1} = 2.05 \times 10^6\,\mathrm{rad \cdot m^{-1}} \\ k_{x,m=1} = |k_{core}| \sin\theta_{i,2} = 1.93 \times 10^6\,\mathrm{rad \cdot m^{-1}} \end{cases} \tag{36}$$

and effective refractive indices of

$$\begin{cases} \mathbf{n_{eff,m=0}} = |k_{core}| \sin\theta_{i,1} = \mathbf{1.52} \\ \mathbf{n_{eff,m=1}} = |k_{core}| \sin\theta_{i,2} = \mathbf{1.43} \end{cases} \tag{37}$$

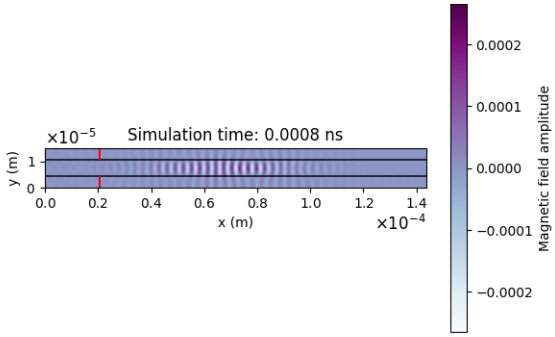

Figure 11: Screenshot of the pulse propagating through the described 2-mode horizontal optical fiber

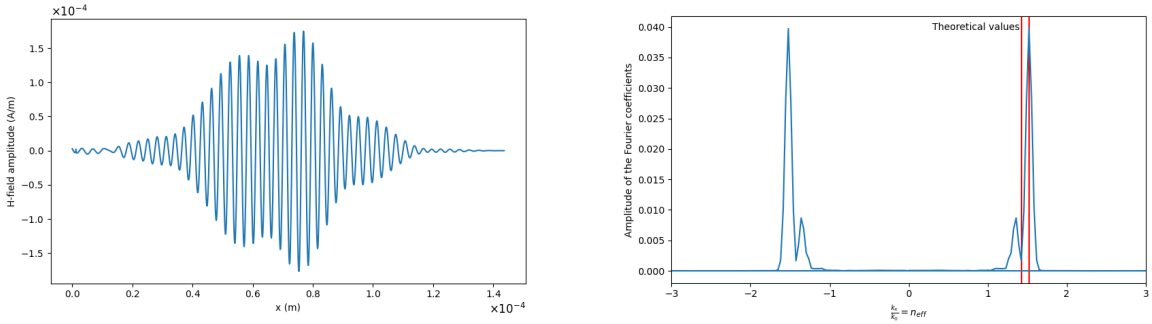

Figure 12: H_z value as a function of x in the fiber (left) and its FFT re-scaled to show the effective refractive index felt by each mode, with a red line for the theoretical values (right)

After applying the FFT to the field in the x-direction, the following results are obtained:

The resolution of the peaks is high for 2 modes, too, yielding two main modes as expected, with a value of k_x:

$$\begin{cases} k_{x,m=0} = |k_{core}| \sin\theta_{i,m=0} = 2.05 \times 10^6 \,\mathrm{rad \cdot m^{-1}} \\ k_{x,m=1} = |k_{core}| \sin\theta_{i,m=1} = 1.84 \times 10^6 \,\mathrm{rad \cdot m^{-1}} \end{cases} \tag{38}$$

and effective refractive indices of

$$\begin{cases} \mathbf{n_{eff,m=0}} = |k_{core}| \sin\theta_{i,m=0} = \mathbf{1.52} \\ \mathbf{n_{eff,m=1}} = |k_{core}| \sin\theta_{i,m=1} = \mathbf{1.36} \end{cases} \tag{39}$$

The achieved result through the FDTD method agrees with the theoretical values within a 0.13% error for the mode with $m = 0$, and within a 4.90% error for the mode with $m = 1$, which is really good.

The shifted peak has a much lower amplitude. ESPECULA !!!

4.3 Dispersion analysis

tell me inputs $(w0, sigma_w)$

First single mode, $m_max = 1$, tell me h, and all solutions of eq 24 for m=0 and m=1. Does it match?

Then 2 modes, and 3 modes. Find necessary m_max

4.4 Bent waveguides

4.4.1 ~~Single-mode bent fiber~~

Results for same parameters as in section **REFERENCE SECTION 4.2.1 SINGLE-MODE OPTICAL FIBER** with the 90° turn, measuring the integral of the Poynting vector across many time iterations to measure the energy propagating through the first, horizontal section, vs the second, vertical section, to see relative propagating intensity after the turn in terms of the radius of curvature. This in turn shows optimal relative radius of curvature

Also, FFT will be performed again but now in the vertical section to see if modes are maintained and when their Fourier amplitude goes below a certain threshold.

5 Conclusion

A more general, greater in size analysis could be performed with a supercomputer

2D simulation, not bad, but not real. Not infinite slab waveguides in practice. This could be generalised to 3D (rectangular waveguides).

Cladding everywhere, good approximation but not realistic.

Attempts could be made to found better, more accurate absorbing boundary conditions.

References

[Agrawal, 2010] Agrawal, G. P. (2010). *Fiber-Optic Communication Systems*. Wiley.

[Born and Wolf, 2013] Born, M. and Wolf, E. (2013). *Principles of optics: electromagnetic theory of propagation, interference and diffraction of light*. Cambridge University Press.

[Clayton and Simpson, 1987] Clayton, C. E. and Simpson, R. J. (1987). Germanium dioxide as a core material for optical fibres. *Electronics Letters*, 23(22):1187–1188.

[Ghatak and Thyagarajan, 1997] Ghatak, A. and Thyagarajan, K. (1997). *Fiber Optics and Optoelectronics*. Cambridge University Press.

[Griffiths, 1999] Griffiths, D. J. (1999). *Introduction to Electrodynamics*. Prentice Hall, Upper Saddle River, NJ, 3rd edition.

[Hecht, 2017] Hecht, E. (2017). *Optics*. Pearson, 5th edition.

[Henderson et al., 2006] Henderson, B., Sazio, P.-J., Peacock, A. C., and Healy, N. (2006). Optical fibers for mid-infrared transmission: materials and fabrication methods. *Sensors and Actuators A: Physical*, 135:44–50.

[Keiser, 2011] Keiser, G. (2011). *Optical Fiber Communications*. McGraw-Hill, 4th edition.

[Maclaurin, 1990] Maclaurin, G. J. (1990). A note on oscillating gaussians. *Journal of Physics A: Mathematical and General*, 23(14).

[Marcuse, 1989] Marcuse, D. (1989). Investigation of coupling between a fiber and an infinite slab. *Journal of Lightwave Technology*, 7(1).

[Okamoto, 2022] Okamoto, K. (2022). *Fundamentals of Optical Waveguides*. Elsevier.

[Scipy community, 2021] Scipy community (2021). Scipy v1.7.1 Reference Guide. `https://docs.scipy.org/doc/scipy/reference/generated/scipy.optimize.brentq.html` Accessed: 2023-03-28.

[Wei et al., 2017] Wei, W., Li, H., Tian, Y., Yang, M., Wang, X., Sun, J., Xie, G., and Zhang, X. (2017). Fluorinated ethylene propylene (fep) as a high-index optical fiber cladding material for humidity sensing. *Journal of Materials Chemistry C*, 5(43):11348–11354.

[Yee, 1966] Yee, K. S. (1966). Numerical solution of initial boundary value problems involving maxwell's equations in isotropic media. *IEEE Transactions on Antennas and Propagation*, 14(3):302–307.

$$\vec{S} = \vec{E} \times \vec{H} = \begin{vmatrix} i & E_x & H_x \\ j & E_y & H_y \\ k & E_z & H_z \end{vmatrix} = \begin{pmatrix} E_y H_z - E_z H_y \\ E_z H_x - E_x \cdot H_z \\ E_x H_y - E_y H_x \end{pmatrix}$$

$$= \begin{pmatrix} E_y H_z \\ -E_x \cdot H_z \\ 0 \end{pmatrix}$$

$$E = \int \left(\iint \vec{S} \cdot d\vec{S} \right) dt$$

$$\simeq \sum_{i \cdot dt} \left(\iint \vec{S} \cdot d\vec{S} \right) \cdot dt$$

$$= \sum_{i \cdot dt} \left[\iint \begin{pmatrix} S_x \\ S_y \\ S_z \end{pmatrix} \cdot \begin{pmatrix} 1 \\ 0 \\ 0 \end{pmatrix} dy\, dz \right] dt$$

$$= \sum_{i \cdot dt} \left[\iint S_x \, dy \, dz \right] \cdot dt$$

take arbitrary z-direction integration

$$\simeq \sum_n \left(\sum_j E_y^n(x_0, j) \cdot H_z^n(x_0, j) \cdot ds \right) \cdot dt$$

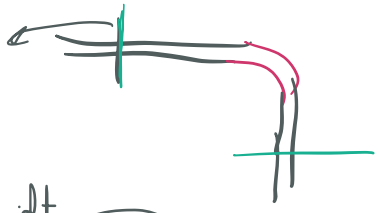

$$= \sum_n \left[\iint \begin{pmatrix} S_x \\ S_y \\ S_z \end{pmatrix} \cdot \begin{pmatrix} 0 \\ -1 \\ 0 \end{pmatrix} dx\, dz \right] dt$$

take arbitrary

$$= \sum_n \left[\int E_x^n \cdot H_z^n \, dx \right] dt$$

$$\simeq \sum_n \left(\sum_i E_x^n(i, y_0) \cdot H_z^n(i, y_0) \, ds \right) dt$$

$$= ds \cdot dt \left(\sum_{i,n} E_x^n(i, y_0) \cdot H_z^n(i, y_0) \right)$$

is this true?